Review of Scientific Instruments

Fast modulating electron cyclotron emission (FMECE) diagnostic for tokamaks

Cite as: Rev. Sci. Instrum. **92**, 033510 (2021); https://doi.org/10.1063/5.0043761
Submitted: 11 January 2021 . Accepted: 16 February 2021 . Published Online: 03 March 2021

Saeid Houshmandyar, Ruifeng Xie, Max E. Austin, William L. Rowan, and Hailin Zhao

Review of Scientific Instruments ARTICLE scitation.org/journal/rsi

Fast modulating electron cyclotron emission (FMECE) diagnostic for tokamaks

Cite as: Rev. Sci. Instrum. 92, 033510 (2021); doi: 10.1063/5.0043761
Submitted: 11 January 2021 • Accepted: 16 February 2021 •
Published Online: 3 March 2021

Saeid Houshmandyar,[1,a)] Ruifeng Xie,[1] Max E. Austin,[1] William L. Rowan,[1] and Hailin Zhao[2]

AFFILIATIONS

[1] Institute for Fusion Studies, The University of Texas at Austin, Austin, Texas 78712, USA
[2] Institute of Plasma Physics, Chinese Academy of Sciences, Hefei 230031, China

Note: Paper published as part of the Special Topic on Proceedings of the 23rd Topical Conference on High-Temperature Plasma Diagnostics.
[a)] **Author to whom correspondence should be addressed:** houshmandyar@austin.utexas.edu

ABSTRACT

Utilizing variable-frequency channels, e.g., yttrium iron garnet (YIG) bandpass filters, in the intermediate frequency (IF) section of an electron cyclotron emission (ECE) radiometer facilitates flexibility in the volume viewed by the ECE channels as well as high resolution electron temperature and temperature fluctuation measurements in tokamaks. Fast modulating electron cyclotron emission (FMECE), a stand-alone IF section with eight channels, is a novel application of YIG filters for real-time electron temperature gradient and gradient scale length measurements. Key to FMECE is a simultaneous input/output data acquisition unit, as well as a modified type of YIG filters, which is capable of fast switching of their center (set) frequencies with a frequency slew rate of 600 μs/GHz. A new FMECE has been implemented and tested on the DIII-D tokamak, demonstrating its capability in real-time gradient measurements. The data presented here shows that FMECE can identify flattening in the electron temperature profile; the latter can be used as a sensor for real time monitoring and control of plasma instabilities. Implementation and application are planned for the EAST tokamak.

I. INTRODUCTION

Electron cyclotron emission (ECE) radiometry is a popular and important diagnostic for contemporary tokamaks because it efficiently measures the profiles of electron temperature (T_e) and electron temperature fluctuations (δT_e) with high spatial and temporal resolution.[1] The excellent photon statistics from the EC emission in tokamaks eases the selection choice of intermediate frequency (IF) channels' bandwidth. Thus, using narrow bandwidth channels in the IF section would enhance the spatial resolution of ECE measurements. Using yttrium iron garnet (YIG) bandpass filters in the IF section has been reported to increase the spatial resolution of the T_e-profile[2] and sensitivity for T_e-fluctuation[3] measurements. In an earlier work,[4] we explored the novel application of fast frequency switching of the YIG filters for measuring the electron temperature gradient scale length ($L_{Te} = T_e/\nabla T_e$). Here, we further this research and development by assembling the fast modulating/mobile ECE (FMECE) diagnostic, which is capable of acquiring the T_e-profile, if calibrated, or a *proxy* for gradient scale length measurements at eight different radii in a calibration-free approach. Not only is it designed to measure real-time gradient but also, if needed, FMECE can cluster the eight ECE channels within the region of interest to increase the spatial resolution of the T_e-profile and ∇T_e measurements. These two characteristics of FMECE are significant in the plasma control context as they have potential to provide enough information to the plasma control actuators, e.g., electron cyclotron current drive (ECCD) for control of the neoclassical tearing modes.[5]

This paper is constructed in four sections. Section II describes the details of the FMECE design and performance, along with the lab testing for spatial and temporal resolution characterization of each channel. The *mobility* feature of FMECE facilitates integrating to any ECE radiometer. This capability enabled testing it at the DIII-D tokamak; the results are shown in Sec. III. The summary and future work are discussed in Sec. IV.

II. THE DIAGNOSTIC DESIGN

FMECE utilizes eight YIG bandpass filters, each custom-designed from Micro Lambda (model MLFP-1710PD) that is tunable between 3.75 GHz and 20 GHz. Special winding by the vendor

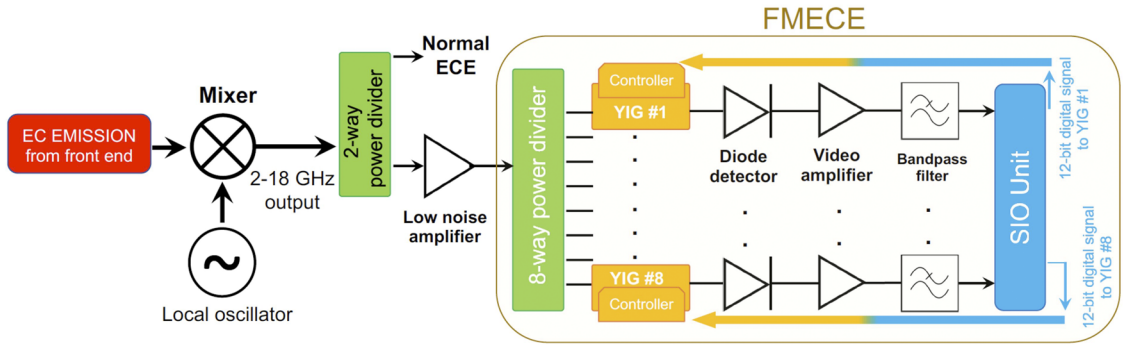

FIG. 1. Schematics of the FMECE diagnostics.

facilitates the fast 600 μs/GHz frequency switching (slew) rate. The signal from each YIG filter is rectified by a Schottky detector, amplified, and then low-pass filtered (250 kHz) before being digitized. Figure 1 shows the schematic of the FMECE diagnostic. An eight-way power divider splits the input ECE signal for the FMECE from the lowest IF band [81 GHz–114 GHz and off the 81 GHz local oscillator (LO)] of the DIII-D's ECE radiometer (HRECE).[2] The signal from each FMECE channel is then digitized by a National Instrument (NI) PXI-7853R simultaneous input/output (SIO) data acquisition (DAQ) with 8 analog and 96 digital channels. An NI PXIe-8301 enables laptop control over a Thunderbolt connection. An NI PXIe-1071 chassis was used for the SIO enclosure, as well as providing power and connection between the laptop and the NI modules. All the programming is in LabView to simultaneously control and acquire data from each FMECE channel. The frequency waveform was applied to the controller of each YIG filter through a 12-bit digital word using the digital channels of the SIO unit. The analog channels of the SIO unit can be digitized with a maximum digitation rate of 700 kHz.

The characteristics of each YIG filter were studied separately and prior to assembling the diagnostic. Using a Keysight MXG-N5183B signal generator and a Keysight MXA N9020B signal analyzer, the 3-dB bandwidth of each filter at a set (center) frequency was measured. As shown in Fig. 2, the bandwidth of each channel is dependent on the set frequency and varies between 120 MHz and 290 MHz.

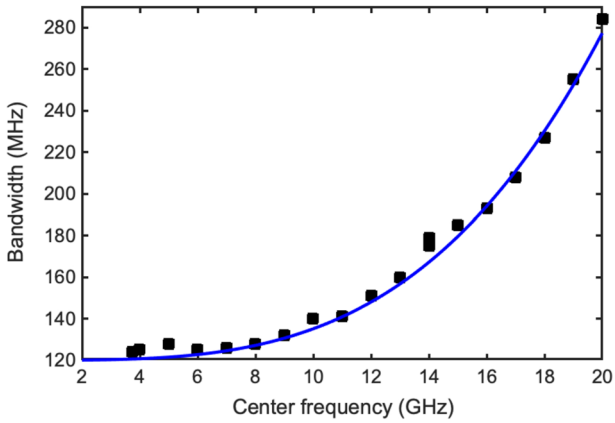

FIG. 2. An example of the frequency dependence of the bandwidth of the YIG filters.

III. ELECTRON TEMPERATURE GRADIENT SCALE LENGTH MEASUREMENTS

Measuring the electron temperature gradient ($\nabla T_e \approx \Delta T_e/\Delta R$) and the electron temperature gradient scale length ($L_{Te}^{-1} = \nabla T_e/T_e$) through the ECE channels requires calibrated ECE data, as well as mapping of the ECE channels within the plasma. The latter can be found via the relation $\Delta R = -R_{i0}\,\Delta f/f_{i0}$, where R_{i0} is the plasma view major radius of the ith ECE channels with its f_{i0} (sum of the local oscillator's and the ith channel frequencies, $f_i + f_{LO}$) frequency. The fast frequency slew rate of the FMECE channels enables a calibration-free scheme for a proxy to the electron temperature gradient scale length measurement. Since the throughput of the YIG filters is constant for small frequency changes, for two close-by frequencies $f_i = f_1$ and f_2, the inverse gradient scale length can be written as

$$L_{Te}^{-1} = \frac{\nabla T_e}{T_e} \approx \frac{1}{\Delta R}\frac{\Delta T_e}{\overline{T_e}} \propto \frac{\Delta f}{|\Delta f|}\frac{\Delta ECE}{\overline{ECE}}. \quad (1)$$

Here, ΔECE is the difference of signal with respect to $\overline{ECE}$, the mean value [the dashed line in Fig. 3(a)], in each cycle of slew and when they are set to slew between frequencies f_1 and f_2, and $\Delta f = f_2 - f_1$ is the frequency change. The right-hand side of Eq. (1) is called the *fractional change*,[6] and it is positive due to the $\Delta f \times \Delta ECE$ factor, unless Δf and ΔECE are opposite in sign. Also note that the fractional change has the opposite sign of the gradient (or the gradient scale length) as $\Delta R \propto -\Delta f$. Figure 3 shows an example of the signal of FMECE's channel 4 when its frequency was slewed between 9.5 GHz and 9.6 GHz ($\Delta f = 0.1$ GHz slew), with 1 ms slew rate; mixed with the local oscillator (LO) with 81 GHz frequency, the channel was slewed between 90.5 GHz and 90.6 GHz of the second ECE harmonic. As mentioned before, there is a trade-off between the higher frequency slew and the temporal resolution; additionally, the assumption of equal throughput for small Δf may not hold for higher frequency slews.

The data shown in Fig. 3 are from FMECE channel 4 when it was tested for a DIII-D discharge 183 547. Note that the frequency setting of this channel would set the channel at $\rho \sim 0.751$. The time

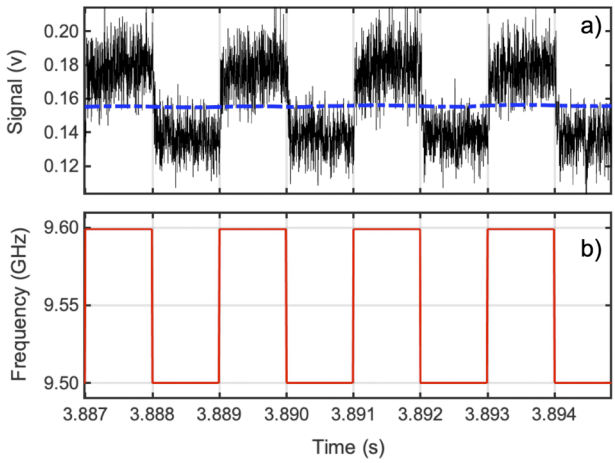

FIG. 3. Eight milliseconds of (a) signal of FMECE channel 4 when (b) it was slewed between 9.5 GHz and 9.6 GHz. The dashed line in the top panel is the mean value of the signal ($\overline{ECE}$).

histories of the plasma parameters for that discharge are shown in Fig. 4. This discharge is predominantly heated by neutral beam injection (NBI) in a hydrogen plasma with B_0 = 2.03 T. Resonant magnetic perturbations (RMPs) coils were used for the intent of L–H transition studies and for edge localized mode (ELM) suppression

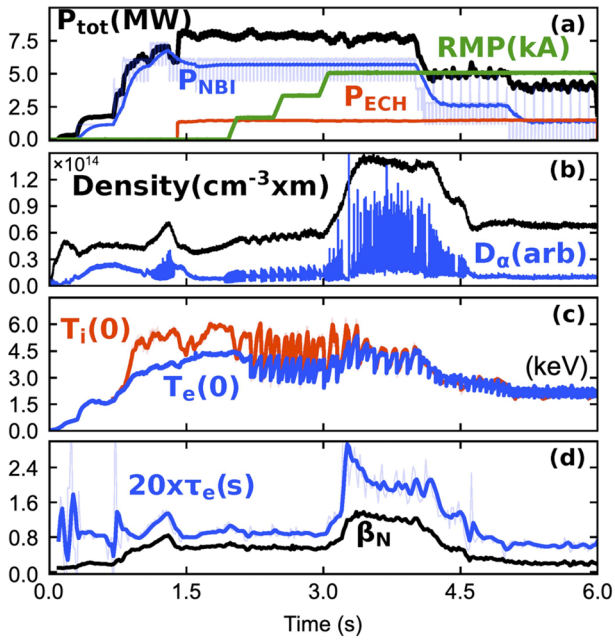

FIG. 4. Time histories of the plasma parameters of the DIII-D shot 183 547. (a) Neutral beam injection (NBI), electron cyclotron heating (ECH), and the total heating powers (in MW units). The current of the RMP coil is shown in kA units. (b) Line averaged density and the divertor D_α showing the ELMs as the discharge transitions to H-mode. (c) Core ion and electron temperatures in keV units. (d) Energy confinement time (multiplied by 20) and the normalized β.

in hydrogen plasmas. The discharge transitioned from L-mode to a dithering H-mode at t = 1.5 s. RMP coils were energized at t = 2.0 s and reached to their maximum at t = 3.0 s when the discharge transitioned into full H-mode with high density and temperatures, and thus higher performance. As the NBI sources turn off, the discharge transitioned back to L-mode at t = 4.5 s. Figure 5(a) shows the electron temperature profiles for the discharge shown in Fig. 4. These profiles are modified hyperbolic tangent (MTANH) fits[7] to the Thomson Scattering (TS) data, and they are plotted vs ρ, which is the normalized toroidal flux function. Pedestal formation—one signature of H-mode discharges—is clearly observed for 1.5 s < t < 4.5 s. Also shown in Figs. 5(b) and 5(c) are the gradient and the inverse gradient scale length, calculated from the fits shown in Fig. 5(a) for 0.65 < ρ < 0.85.

The T_e-profiles from ECE diagnostic are found to be in good agreement with the profile fits to the TS diagnostic data [shown in Fig. 5(a)]. Figure 6 shows the edge region of T_e-profiles measured by the ECE diagnostics at three different times. These traces are plotted (bottom x-axis) vs the frequencies associated with the second ECE harmonic ($f_{2\mathrm{ECE}}$), where $f_{n\mathrm{ECE}} = n \times 2.8 \times 10^8 B$ for the nth harmonic and B (= B_0R_0/R_{vac}) is the local magnetic field strength. R_{vac} is the corresponding ECE viewing radius in vacuum, and B_0 is the magnetic field at magnetic axis R_0. In addition, for each plot, the top x-axis is the normalized toroidal flux function (ρ) for the given time. In particular, the standard analysis used here for the ECE measurements is well known to erroneously show increased electron temperatures beyond the last closed flux surface (LCFS) (e.g., Ref. [8]). Different mechanisms such as reflections off the walls and radiation from the non-thermal electrons contribute to this increase.

However, most importantly, these measurements do not reflect electron temperature as these channels collect EC emission from a region in plasma that is not "optically thick"; the latter is the requirement for valid ECE measurements. Thus, the ECE

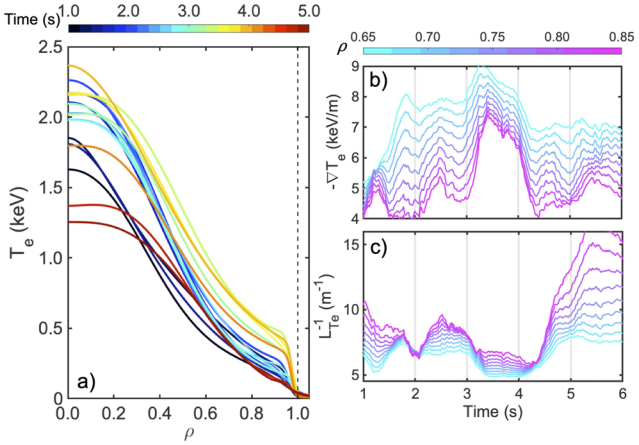

FIG. 5. (a) A few traces of the electron temperature profile of the discharge shown in Fig. 4. Each trace is a fit to the Thomson scattering data at different times, and each time is identified in the color bar (b) Time evolution of the electron temperature gradient and (c) electron temperature inverse gradient scale length at different ρ values, where the ρ values are shown in the color bar.

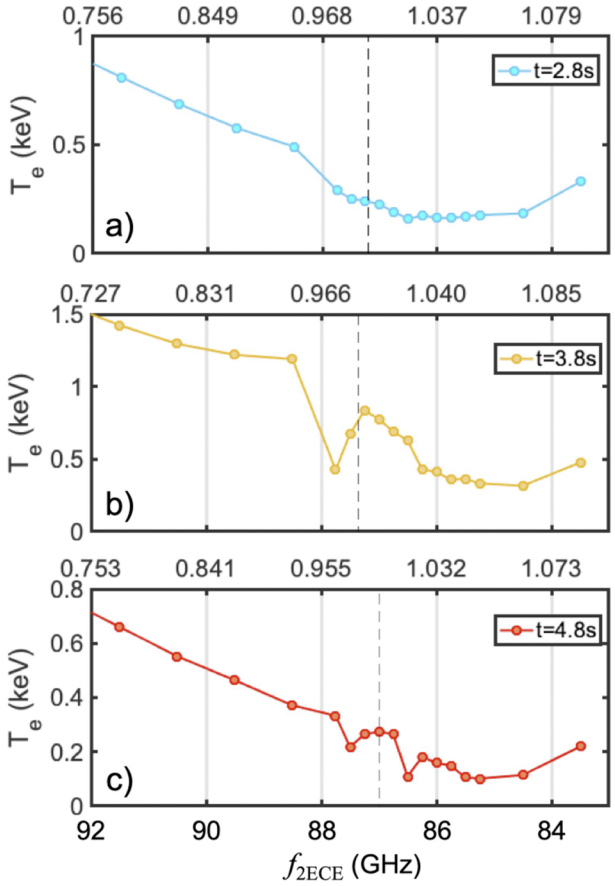

FIG. 6. Electron temperature profiles in the edge region measured by the ECE diagnostic vs (bottom x-axis) second ECE harmonic frequencies at (a) t = 2.8 s, (b) t = 3.8 s, and (c) t = 4.8 s. The color for each trace is matched with those in Fig. 5(a). The top x-axis in each plot is the ρ value calculated from the reconstructed equilibria, and the vertical dashed line marks the $\rho = 1$ location.

channels with frequencies $f_{2ECE} < 87.5$ GHz were not measuring electron temperature. For the times (e.g., $t = 3.8$ s in Fig. 4) when the discharge transits into full H-mode, this frequency threshold was 87.75 GHz.

The moving of the LCFS with respect to the ECE channels can be due to plasma displacement at higher NBI powers and/or their net torque or, in this case, an effect from the RMP. Regardless of the reasons for this moving, the T_e-gradient would be inferred to be positive (or negative fractional change) if the gradient calculation is performed between two channels that are measuring ECE beyond the LCFS. Evidently, the positive gradient (or the negative fractional change) would be an incorrect illustration of ∇T_e. Figure 7(a) shows an example of the evolution of the fractional change calculated from the ECE diagnostic. Here, ΔT_e is the temperature difference, calculated from two channels of the ECE diagnostic with frequencies 87.5 GHz and 87.75 GHz, and $\overline{T_e}$ is the mean value of the temperatures of the two channels. As discussed earlier, for 3.0 s < t < 4.5 s, and when the discharge was in full H-mode, these two channels would measure ECE from the non-optically thick region (e.g., $t = 3.8$ s), which would result in the negative fractional change. Figure 7(b) shows the fractional change measurement from FMECE channel 1 when it was set to slew between 87.5 GHz and 87.6 GHz with 1 ms slew rate. Similar to Fig. 7(a), the fractional change is negative when the discharge was in full H-mode. This shows that FMECE and the regular ECE observe the same phenomenon when they have the same settings.

Shown in Fig. 7(c) is the fractional change measurement between two ECE channels with frequencies 89.5 GHz and 90.5 GHz. Figure 7(d) shows fractional change measurement from FMECE channel 4 when it was set to slew between 90.5 GHz and 90.6 GHz with 1 ms slew rate. Likewise, Figs. 7(c) and 7(d) show reduction in the fractional change for 3.0 s < t < 4.5 s when the discharge was in full H-mode. The trend is consistent with the one in L_{Te}^{-1} calculated from the TS data [shown in Fig. 5(b)] at $\rho \sim 0.8$ in which decrease in the scale length is observed at $t \sim 3.0$ s.

It should be emphasized that there is not a one-to-one correlation between Figs. 7(a) and 7(b) [and similarly, Figs. 7(c) and 7(d)] as the frequency steps (slew) are not the same (1 GHz vs 0.1 GHz). Moreover, the ECE calibration is included in the calculations shown in Figs. 7(a) and 7(c) while the measurement shown in Figs. 7(b) and 7(d) is calibration-free. Alternatively, one would contrast this dissimilarity as average-versus-local gradient comparison. However, the results from Fig. 7 suggest that the technique is yielding a proxy for L_{Te}^{-1}, and this proxy can be used as a sensor for control purposes. For example, the reduction in the fractional change from multiple channels is a representative of T_e-profile flattening, which is also the hallmark of magnetic islands. Real-time clustering of the FMECE

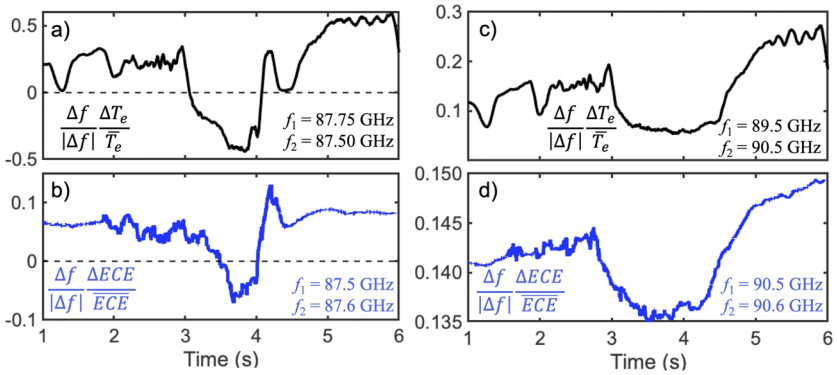

FIG. 7. Comparison of the fractional change calculated from the profiles measured by the ECE diagnostics [(a) and (c)] and those measured by FMECE (b) channel 1 and (d) channel 4. Each trace is the moving average value with the 100 ms time window.

channels on to a specific region[9] (e.g., the island region) can provide information on the island size and dynamics and ultimately, enhancing the "catch and subdue" algorithm for NTM control.[10]

IV. SUMMARY

This paper presents the details and performance of the fast modulating/mobile electron cyclotron emission (FMECE) diagnostic. FMECE is an eight-channel IF unit that can be integrated to any ECE radiometer and is capable of real-time measuring of the "fractional change," ($\Delta ECE/\overline{ECE}$), which is a proxy to the electron temperature gradient scale length ($L_{Te}{}^{-1} = \nabla T_e/T_e$). This capability is facilitated by utilizing eight yttrium iron garnet (YIG) bandpass filters and a SIO data acquisition unit. The special design of the YIG filters provided by the vendor enables fast frequency switching for the YIG filters and hence fractional change measurements with 0.6 ms temporal resolution at eight different major radial locations. These results show that FMECE can effectively identify flattening in the electron temperature profile and monitor magnetic islands' dynamics. FMECE is planned to be integrated to the radiometer at the EAST tokamak to potentially predict locked modes via monitoring island size prior to the locked mode events.

ACKNOWLEDGMENTS

This work was supported by U.S. Department of Energy OFES under Award Nos. DE-FG02-97ER54415, DE-FC02-04ER54698, and DE-SC0010500. The OMFIT integrated modeling framework[11] was used for the data analysis of this work.

DATA AVAILABILITY

The data that support the findings of this study are available from the corresponding author upon reasonable request.

REFERENCES

[1] C. Watts, Fusion Sci. Technol. **52**, 1176 (2007).
[2] D. D. Truong and M. E. Austin, Rev. Sci. Instrum. **85**, 11D814 (2014).
[3] M. Fontana, L. Porte, and P. Molina Cabrera, Rev. Sci. Instrum. **88**, 083506 (2017).
[4] S. Houshmandyar, M. E. Austin, M. W. Brookman, Y. Liu, W. L. Rowan, and H. Zhao, Rev. Sci. Instrum. **89**, 10H109 (2018).
[5] E. Kolemen, R. Ellis, R. J. La Haye, D. A. Humphreys, J. Lohr, S. Noraky, B. G. Penaflor, and A. S. Welander, Fusion Eng. Des. **88**, 2757 (2013).
[6] S. Houshmandyar, Z. J. Yang, P. E. Phillips, W. L. Rowan, A. E. Hubbard, J. E. Rice, J. W. Hughes, and S. M. Wolfe, Rev. Sci. Instrum. **87**, 11E101 (2016).
[7] R. J. Groebner *et al.*, Nucl. Fusion **41**, 1789 (2002).
[8] S. S. Denk *et al.*, Plasma Phys. Controlled Fusion **60**, 105010 (2018).
[9] R. Xie, S. Houshmandyar, and M. E. Austin, Rev. Sci. Instrum. (to be published 2021).
[10] E. Kolemen, A. S. Welander, R. J. La Haye, N. W. Eidietis, D. A. Humphreys, J. Lohr, V. Noraky, B. G. Penaflor, R. Prater, and F. Turco, Nucl. Fusion **54**, 073020 (2014).
[11] O. Meneghini *et al.*, Nucl. Fusion **55**, 083008 (2015).